Dalton Transactions

ROYAL SOCIETY OF CHEMISTRY

COMMUNICATION

View Article Online
View Journal | View Issue

Cite this: *Dalton Trans.*, 2024, **53**, 7263

Received 27th December 2023,
Accepted 26th March 2024

DOI: 10.1039/d3dt04352e

rsc.li/dalton

Magnetic anisotropy in octahedral Dy(III) and Yb(III) complexes†

Aditya Borah, [a,c] Sourav Dey, [a] Kehkasha Siddiqui, [a] Sandeep K. Gupta, [b] Gopalan Rajaraman *[a] and Ramaswamy Murugavel *[a]

New organophosphate complexes $[Ln(dippH)_3(dippH_2)_3]\cdot(H_2O)_6$, (Ln = Dy, Yb and Y; $dippH_2$ = 2,6-diisopropylphenyl phosphate), displaying octahedral coordination geometry around the metal ion, exhibit unusual slow relaxation of magnetisation, which is investigated through experimental studies and *ab initio* CASSCF calculations.

Molecular systems showing slow relaxation of magnetization due to magnetic bistability are called single-molecule magnets (SMMs).[1] Since this phenomenon is purely molecular in origin, it has potential applications in magnetic storage devices[2] and spintronics.[3–5] The energy barrier for magnetization reversal (U_{eff}) and the blocking temperature (T_B) below which the opening of magnetic hysteresis is observed are considered to be figures of merit for SMMs.[6–8] In this regard, late lanthanides, particularly Dy(III), based SMMs have drawn particular attention in the past two decades because their large magnetic anisotropy originating from the strong spin–orbit coupling of the metal centre that leads to the very high U_{eff} for magnetization reversal.[9,10] The ligand field (LF) around the Ln(III) centre plays a very crucial role towards the SMM behaviour, though the interaction of the LF with the 4f electrons is very weak.[11–14] The linear two-coordinated ligand field around the metal is found to be ideal for achieving higher U_{eff} and T_B values as this geometry allows the complex to relax *via* the highest excited state, nullifying the existence of quantum tunnelling of magnetization (QTM).[15] Unlike the linear two-coordinated transition metal analogues, synthesis of low-coordinated lanthanide complexes is very difficult owing to the large ionic radii of Ln(III) ions.[16] In the past six years, we have witnessed the axial limit of magnetic anisotropy in which the metal centre like Dy resides in an axially compressed high symmetry ligand field (D_{4h},[17,18] D_{5h},[19–27] D_{6h},[28,29] D_{8h} [30,31]). While a strong axial ligand field and weak/no equatorial ligand field are required to stabilize the ground oblate electron density, a reverse ligand field is essential to stabilize the ground prolate electron density.[32,33] However, both oblate and prolate-shaped electron clouds are expected to be isotropic once the ion is in an LF of perfect octahedral symmetry.

Herein, we report three mononuclear Ln(III) complexes $[Ln(dippH)_3(dippH_2)_3]\cdot(H_2O)_6$ (Ln = Dy **1**; Yb **2** and Y **3**) based on a bulky organophosphate, 2,6-diisopropyl phenyl phosphate ($dippH_2$), where six of these $dippH_2$ ligands create a nearly perfect octahedral ligand field around the central Ln(III) ions. The main objective of this work is to investigate whether ions with oblate or prolate-shaped electron clouds become isotropic once they are placed in a spherical LF. Two extreme ions Dy (for oblate) and Yb (for prolate) are taken into consideration, and this work shows that both these complexes possess significant magnetic anisotropy.

Compounds **1–3** have been synthesized from the reaction of the respective hydrated Ln(III) nitrate with $dippH_2$ under ambient conditions as shown in Scheme 1. Organophosphate ligands ($R/Ar\text{-}OPO_3H_2$) are best known for yielding clusters or polymeric networks, due to the presence of three oxygen atoms available for coordination per ligand.[34–36] The affinity of phosphate ligands to behave as multidentate ligands is ceased by performing the reaction in the absence of any base so that

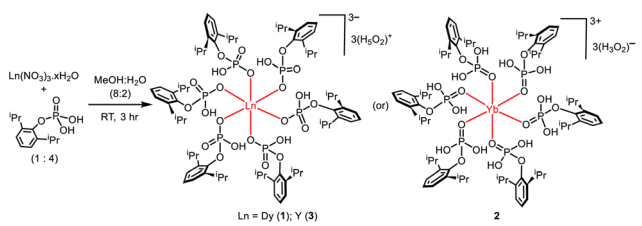

Scheme 1 Synthesis of **1–3**.

[a]*Department of Chemistry, Indian Institute of Technology Bombay, Powai, Mumbai, Maharashtra, 400076, India. E-mail: rmv@chem.iitb.ac.in*
[b]*Department of Chemistry, Indian Institute of Technology Delhi, Hauz Khas, Delhi, 110016, India*
[c]*Department of Chemistry, Jengraimukh College, Majuli, Assam, 785105, India*

†Electronic supplementary information (ESI) available. CCDC 2069003, 2069009 and 2331545. For ESI and crystallographic data in CIF or other electronic format see DOI: https://doi.org/10.1039/d3dt04352e

deprotonation of the acid is restricted. This strategy yields mononuclear six-coordinated Ln(III) hexaphosphate complexes. To the best of our knowledge, these are the first Ln(III) based coordination compounds with octahedral symmetry that contain six phosphates. The strong absorption peaks in the FTIR spectra of **1–3** in the regions of 1200–1150 cm^{-1} and 1000–850 cm^{-1} are due to the presence of P=O stretching and M–O=P symmetric and asymmetric vibrations, respectively. The broad absorption peak centred at 2300 cm^{-1} confirms the presence of the free P–OH group of the $dippH_2$ ligands, while the broad peak near 3500 cm^{-1} originates from lattice $(H_5O_2)^+$/$(H_3O_2)^-$ moieties (*vide infra*, Fig. S1†).

Single crystal X-ray structure analysis of isomorphous **1–3** reveals that the asymmetric part of the $R\bar{3}$ unit cell contains one-sixth of the Ln(III) ion, an organophosphate, and a lattice water molecule (Fig. 1; also see Table S1 and Fig. S6–S8†). The full molecule contains the respective Ln(III) centre and six $dippH_2$ ligands coordinating the Ln(III) centre *via* P–O–Ln coordination along with six lattice water molecules. The lattice $H_3O_2^-$ ions are close enough to the organophosphate $dippH_2$ to enable the shuttling of the acidic proton H3 to-and-fro between O3 and O5 of the anion, thus converting $dippH_2$ to $dippH^-$ and $(H_3O_2)^-$ to $(H_5O_2)^+$. These two extremes are observed in **1**, **3** ($(H_5O_2)^+$) and **2** ($(H_3O_2)^-$) (Fig. S8 and S9†). In case of **1** and **3**, H3 in the fully protonated form ($dippH_2$) is closer to O5 (H3–O5: 1.183 Å; H3–O3: 1.353 Å in **1** and H3–O5: 0.852 Å; H3–O3: 1.669 Å in **3**), forming a $dippH^-$ and $(H_5O_2)^+$ ion like situation while, in **2**, H3 is close to O3 (H3–O3: 0.694 Å; H3–O5: 1.842 Å) resulting in an $(H_3O_2)^-$ moiety leaving organophosphate protonated (Scheme 2). Thus, the more accurate molecular formulae turn out to be $[Dy(dippH)_6]\cdot(H_5O_2)_3$ for **1**, $[Yb(dippH_2)_6]\cdot(H_3O_2)_3$ for **2** and $[Y(dippH)_6]\cdot(H_5O_2)_3$ for **3**, at the temperature at which the X-ray diffraction experiments have been performed.

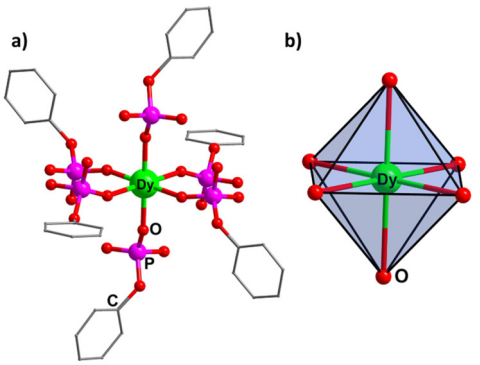

Fig. 1 (a) Molecular structure of **1**. Isopropyl groups on the phenyl ring, H atoms and lattice water molecules are omitted for clarity. (b) Polyhedron showing the O_h symmetry around the Dy(III) ion. Selected structural parameters for **1**: Dy–O = 2.2428(2) Å; O–Dy–O = 87.45(5), 92.55(5) and 180°; for **2**: Yb–O = 2.2016(8) Å; O–Yb–O = 87.85(7), 92.15 (7), and 180°; for **3**: Y–O = 2.2259(1) Å; O–Y–O = 87.60(4), 92.39(4), and 180°.

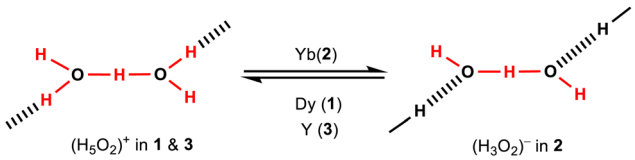

Scheme 2 Proton shuttle producing either $H_5O_2^+$ or $H_3O_2^-$ counter ions.

The continuous SHAPE measurements[37] reveal that the Ln(III) ions occupy a close to perfect octahedral coordination environment (Fig. 1b; and Table S5†). All six Ln–O lengths are equal (2.2428(2) Å for **1**, 2.2016(8) Å for **2** and 2.2259(1) Å for **3**), but the bond angles show a slight deviation in the *cis*-angles (Fig. 1 and Tables S3–S5†). Due to the presence of six free P–OH groups per molecule (twelve in case of **2**), there exists extensive intramolecular (among the ligated phosphates) and intermolecular (between the lattice $(H_5O_2)^+$/$(H_3O_2)^-$ and phosphates) H-bonding (Fig. S10 and S11†). The adjacent molecules in the lattice are well separated with the closest Ln···Ln distance being 14.131(4) Å in **1** and 14.321(1) Å in **2**, which is mainly due to the presence of six bulky phenyl rings per molecule, thus reducing the possibility of any intermolecular magnetic interactions between the nearest neighbours. The phase purity of the samples has been confirmed by powder X-ray diffraction studies of the powdered bulk samples (Fig. S13–S15†).

The magnetic property measurements of **1** and **2** have been carried out on pure polycrystalline powdered samples. The room temperature $\chi_M T$ values are 14.02 cm^3 K mol^{-1} for **1** and 2.64 cm^3 K mol^{-1} for **2**, which are in good agreement with the calculated values for isolated non-interacting Dy(III) ($^6H_{15/2}$, 14.18 cm^3 K mol^{-1}) and Yb(III) ($^2F_{7/2}$, 2.57 cm^3 K mol^{-1}) ions, respectively (Fig. S16†). On cooling, the $\chi_M T$ value for **1** decreases smoothly up to 50 K before suddenly decreasing to 8.98 cm^3 K mol^{-1} at 2 K. The decrease of $\chi_M T$ values in the case of **2** is however smooth over the entire temperature range reaching 0.45 cm^3 K mol^{-1} at 2 K. The non-overlapping nature of field dependence of the magnetization curve at different temperatures indicates the existence of magnetic anisotropy in both **1** and **2** (Fig. S17 and S18†).

The relaxation dynamics of magnetization in **1** and **2** have been explored with the help of alternating current (ac) susceptibility measurements with an oscillating field of 3.5 Oe. Both of the complexes don't show any out-of-phase signal (χ'') even at 1.8 K due to the presence of strong QTM. QTM can be suppressed to the highest extent by the application of a suitable external dc field (Fig. S17 and S18†). Under the optimized dc field (600 Oe for **1** and 1250 Oe for **2**), **1** and **2** show frequency-dependent χ'' peaks up to 5.0 K and 5.8 K, respectively (Fig. 2a for **1** and 2b for **2**). This confirms that both complexes are field-induced SIMs. The relaxation times (τ_0) associated with **1** and **2** are extracted from the fitting of Cole–Cole plots (Fig. S21 and S22†). The plots are well-fitted by considering a single relaxation process (the relaxation times for the unresolvable

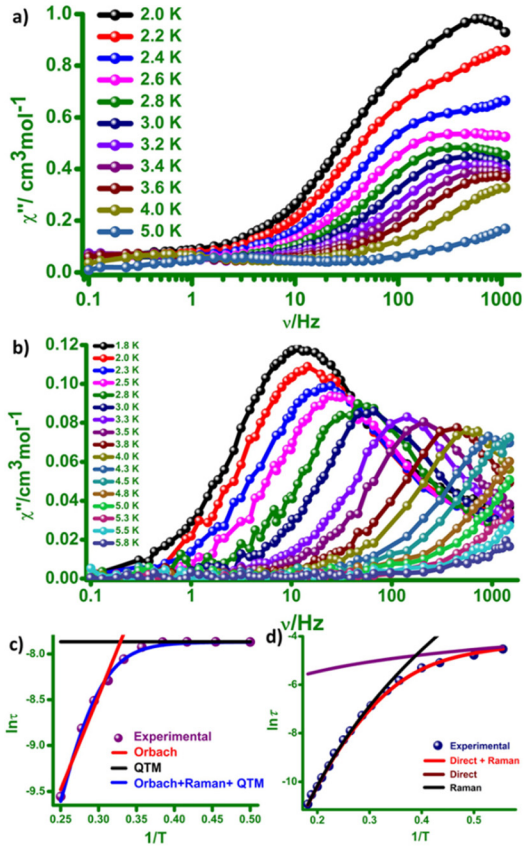

Fig. 2 Frequency dependent out-of-phase (χ'') ac susceptibility signals for (a) **1** and (b) **2** under applied fields of 600 Oe and 1250 Oe, respectively. Arrhenius plot of ln τ *versus* 1/T for (c) **1** and (d) **2**. Red lines represent the best fit by considering the indicated relaxation processes; green, blue, black and purple lines represent data fits by considering the individual contribution from Orbach, QTM, Raman and direct process, respectively.

seemingly second relaxation process in the high frequency region could not be extracted considering two relaxation processes in Cole–Cole fitting), using the generalized Debye function with a wide distribution of relaxation times ($0.32 < \alpha < 0.49$ for **1** and $0.03 < \alpha < 0.25$ for **2**). In the case of **1**, the plot of ln τ_0 *vs.* 1/T contains two clear regimes: a strongly temperature-dependent regime in the higher temperature range (3.0 K–5.0 K) and a temperature-independent regime below 3.0 K. The linear part in the high-temperature regime is fitted with the Arrhenius law, $\tau = \tau_0 \exp(U_{\text{eff}}/k_{\text{B}}T)$, yielding the thermal barrier height of magnetization reversal, U_{eff} = 20.5 K and $\tau_0 = 2.5 \times 10^{-15}$ s. The temperature dependence of τ has been modelled with QTM, direct, Raman and Orbach processes using the equation: $\tau^{-1} = {\tau_{\text{QTM}}}^{-1} + AT + CT^n + {\tau_0}^{-1} \exp(-U_{\text{eff}}/k_{\text{B}}T)$. Best fitting of relaxation time over the whole temperature range using multiple relaxation processes indicates that the relaxation occurs *via* Orbach, Raman and QTM processes with the value of the Raman exponent n = 4 and C = 0.5 s^{-1} K^{-3} (Fig. 2c). To examine whether the magnetisation relaxation is purely molecular in origin or not, an approximately 20% diluted sample of **1** in the matrix of **3** was synthesized (confirmed by ICP-AES, see the ESI†) and both dc and ac magnetic susceptibility measurements were investigated (Fig. S30–S32†). The compound, **1Y**, shows that it relaxes through a single relaxation process with U_{eff} = 17.2 K and $\tau_0 = 3.04 \times 10^{-8}$ s. Interestingly, the second unresolvable relaxation process in the pristine **1**, which might be due to dipolar interactions, is suppressed in **1Y** as only one relaxation is present in the latter case. The barrier height of **1Y** is close to that of **1**, confirming that the single-ion magnetism of **1** is purely molecular in origin.

In the case of **2**, the Arrhenius fit to the linear part of the ln τ *vs.* 1/T plot in the high-temperature regime yields U_{eff} = 33.8 K and $\tau_0 = 1.3 \times 10^{-17}$ s. Several attempts were carried out to fit the non-linear Arrhenius plot. The plot is best fitted by only considering the direct and Raman processes (A = 47.0 s^{-1} K^{-1}, C = 0.057 s^{-1} K^{-n} and n = 8.1), which eliminates the presence of the Orbach process in the relaxation dynamics of **2**. The individual contributions of the Raman and direct processes over the whole temperature range are understood by plotting the individual parameters (Fig. 2d). This demonstrates that the Raman process dominates in the high-temperature region (3.0–5.5 K) while the direct process is dominant in the low-temperature region (1.8–2.0 K). The dominance of the Raman and direct processes over other processes like Orbach and QTM in the relaxation dynamics of Yb(III) based SMMs has been previously observed.[38]

To further investigate the origin of magnetic anisotropy in complexes **1** and **2**, we have performed *ab initio* CASSCF/RASSI-SO/SINGLE_ANISO calculations using MOLCAS8.2. The computed magnetic anisotropy axis of KD1 is found to be oriented along the C_3 axis which is formed by the O═P groups in both complexes (Fig. 3 and S23†). The calculations reveal strong transverse anisotropy in the KD1 (Kramers doublet) of both complexes (**1**: g_{xx} = 9.709, g_{yy} = 8.971 and g_{zz} = 0.330, **2**: g_{xx} = 3.318, g_{yy} = 3.294 and g_{zz} = 1.467, Tables S8 and S9†), leading to strong QTM in the ground state. This implies field-induced SIM behaviour in **1** and **2**, consistent with experi-

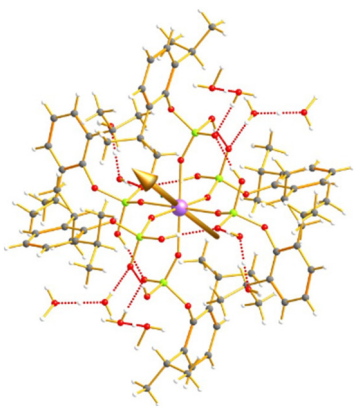

Fig. 3 The magnetic anisotropy axis of complex **1**. Colour code: Dy – purple, O – red, P – green, C – grey, H – white.

mental results. The eight KDs generated from $^6H_{15/2}$ span around 821.3 cm^{-1} in **1** while four KDs from $^2F_{7/2}$ span around 540.7 cm^{-1} in **2** (Tables S8 and S9†). The ground KD of **1** possesses strong mixing between m_J = |±7/2>, |±5/2> and |±1/2> while the same for **2** shows strong mixing between m_J = |±7/2> and |±5/2>, leading to strong QTM (Fig. 4 and S23†). Compared to the Dy complex, the Yb analogue shows less mixing between m_J states leading to smaller QTM in **2** compared to **1**. We have also computed the crystal field parameter according to Stevens Hamiltonian $\hat{H}_{CF} = \sum_{k=2}^{6}\sum_{q=-k}^{k} B_k^q \tilde{O}_k^q$, where B_k^q is the crystal field parameter and $\tilde{O}_k^q$ is the Stevens operator[39] (Table S10†). The large negative value of B_2^0 represents significant magnetic axiality in **2** while it becomes positive in **1**, implying reduced magnetic axiality in **1** compared to **2** (Table S10†). This is also reflected in the higher U_{eff} of **2** compared to **1**. The KD1–KD2 energy gap is estimated to be 34.6 and 157.4 cm^{-1} for **1** and **2**, respectively. This value is slightly overestimated compared to U_{eff} in **1** but strongly overestimated in **2**. The overestimation of U_{cal} compared to U_{eff} is common in Yb(III) based SIMs[17,40–42] and can be explained by the neglect of metal–ligand covalency, which increases from left to right across the lanthanide series. Furthermore, the computed magnetic susceptibility and magnetization were found to agree well with experiment for **1** but deviate significantly from experiment for **2** (Fig. S17–18 and S24†). This can be ascribed to the inherent issues with the method for the Yb(III) ion as the inclusion of dynamic correlation by means of CASPT2 calculations on a few Yb(III) complexes reported by us earlier shows significant deviation of computed data from experiment.[16] However, to investigate the origin of the magnetic anisotropy, we have analysed the LoProp charges of complexes **1** and **2**. Quite interestingly, it has been found that the LoProp charge of one metal-coordinated oxygen atom is different from the others in both **1** and **2** (Table S11 and Fig. S25†). This creates an asymmetric charge distribution around the metal atom, leading to the field-induced SIM behaviour for complexes **1** and **2**.

To conclude, we have synthesized two Ln-organophosphates exhibiting nearly ideal octahedral ligand fields around oblate Dy(III) and prolate Yb(III) ions. *Ab initio* calculations have been employed to uncover the prime cause of the unexpected magnetic behaviour, confirming the presence of strong transverse anisotropy due to the asymmetric charge distribution around Ln(III) ions.

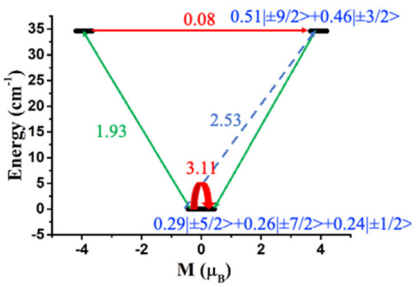

Fig. 4 The mechanism of magnetisation relaxation of complex **1**. The red arrows indicate QTM *via* the ground state and TA-QTM *via* the first excited state. The dotted arrow represents the Orbach process and the green arrows represent the possible mechanism of magnetisation relaxation. The blue characters indicate the m_J composition of KDs.

Conflicts of interest

There are no conflicts to declare.

Acknowledgements

We thank the SERB, New Delhi for funding this work (SB/S2/JCB-2014, SB/SJF/2019-20/12, SPR/2019/001145 and CRG/2022/002406 & 001697).

References

1 R. Sessoli, D. Gatteschi, A. Caneschi and M. Novak, *Nature*, 1993, **365**, 141–143.
2 M. Mannini, F. Pineider, P. Sainctavit, C. Danieli, E. Otero, C. Sciancalepore, A. M. Talarico, M.-A. Arrio, A. Cornia and D. Gatteschi, *Nat. Mater.*, 2009, **8**, 194.
3 M. Urdampilleta, S. Klyatskaya, J.-P. Cleuziou, M. Ruben and W. Wernsdorfer, *Nat. Mater.*, 2011, **10**, 502–506.
4 R. Vincent, S. Klyatskaya, M. Ruben, W. Wernsdorfer and F. Balestro, *Nature*, 2012, **488**, 357–360.
5 S. Thiele, F. Balestro, R. Ballou, S. Klyatskaya, M. Ruben and W. Wernsdorfer, *Science*, 2014, **344**, 1135–1138.
6 C. A. Goodwin, F. Ortu, D. Reta, N. F. Chilton and D. P. Mills, *Nature*, 2017, **548**, 439–442.
7 F.-S. Guo, B. M. Day, Y.-C. Chen, M.-L. Tong, A. Mansikkamäki and R. A. Layfield, *Science*, 2018, **362**, 1400–1403.
8 K.-X. Yu, J. G. Kragskow, Y.-S. Ding, Y.-Q. Zhai, D. Reta, N. F. Chilton and Y.-Z. Zheng, *Chem*, 2020, **6**, 1777–1793.
9 N. Ishikawa, M. Sugita, T. Ishikawa, S.-y. Koshihara and Y. Kaizu, *J. Am. Chem. Soc.*, 2003, **125**, 8694–8695.
10 G. Cucinotta, M. Perfetti, J. Luzon, M. Etienne, P. E. Car, A. Caneschi, G. Calvez, K. Bernot and R. Sessoli, *Angew. Chem., Int. Ed.*, 2012, **51**, 1606–1610.
11 L. Sorace, C. Benelli and D. Gatteschi, *Chem. Soc. Rev.*, 2011, **40**, 3092–3104.
12 S. K. Gupta and R. Murugavel, *Chem. Commun.*, 2018, **54**, 3685–3696.
13 D. N. Woodruff, R. E. Winpenny and R. A. Layfield, *Chem. Rev.*, 2013, **113**, 5110–5148.
14 A. Borah and R. Murugavel, *Coord. Chem. Rev.*, 2022, **453**, 214288.
15 N. F. Chilton, C. A. Goodwin, D. P. Mills and R. E. Winpenny, *Chem. Commun.*, 2015, **51**, 101–103.
16 J. Emerson-King, G. Gransbury, G. Whitehead, I. Vitorica-Yrezabal, M. Rouzières, R. Clérac, N. Chilton and D. Mills, *J. Am. Chem. Soc.*, 2024, **146**, 3331–3342.

17 A. Borah, S. Dey, S. K. Gupta, M. G. Walawalkar, G. Rajaraman and R. Murugavel, *Chem. Commun.*, 2020, **56**, 11879–11882.
18 X. L. Ding, Y. Q. Zhai, T. Han, W. P. Chen, Y. S. Ding and Y. Z. Zheng, *Chem. – Eur. J.*, 2021, **27**, 2623–2627.
19 Y.-C. Chen, J.-L. Liu, L. Ungur, J. Liu, Q.-W. Li, L.-F. Wang, Z.-P. Ni, L. F. Chibotaru, X.-M. Chen and M.-L. Tong, *J. Am. Chem. Soc.*, 2016, **138**, 2829–2837.
20 Y. S. Ding, N. F. Chilton, R. E. Winpenny and Y. Z. Zheng, *Angew. Chem., Int. Ed.*, 2016, **55**, 16071–16074.
21 S. K. Gupta, T. Rajeshkumar, G. Rajaraman and R. Murugavel, *Chem. Sci.*, 2016, **7**, 5181–5191.
22 M. S. Norre, C. Gao, S. Dey, S. K. Gupta, A. Borah, R. Murugavel, G. Rajaraman and J. Overgaard, *Inorg. Chem.*, 2019, **59**, 717–729.
23 A. B. Canaj, S. Dey, O. Céspedes, C. Wilson, G. Rajaraman and M. Murrie, *Chem. Commun.*, 2020, **56**, 1533–1536.
24 S. Dey and G. Rajaraman, *J. Chem. Sci.*, 2019, **131**, 124.
25 P. Kalita, N. Ahmed, A. K. Bar, S. Dey, A. Jana, G. Rajaraman, J.-P. Sutter and V. Chandrasekhar, *Inorg. Chem.*, 2020, **59**, 6603–6612.
26 J. B. Petersen, Y.-S. Ding, S. Gupta, A. Borah, E. J. McInnes, Y.-Z. Zheng, R. Murugavel and R. E. Winpenny, *Inorg. Chem.*, 2023, **62**, 8435–8441.
27 S. K. Gupta, S. Dey, T. Rajeshkumar, G. Rajaraman and R. Murugavel, *Chem. – Eur. J.*, 2022, **28**, e202103585.
28 A. B. Canaj, S. Dey, E. R. Martí, C. Wilson, G. Rajaraman and M. Murrie, *Angew. Chem.*, 2019, **131**, 14284–14289.
29 A. Borah, S. Dey, S. K. Gupta, G. Rajaraman and R. Murugavel, *Dalton Trans.*, 2023, **52**, 8943–8955.
30 L. Ungur, J. J. Le Roy, I. Korobkov, M. Murugesu and L. F. Chibotaru, *Angew. Chem.*, 2014, **126**, 4502–4506.
31 J. J. Le Roy, L. Ungur, I. Korobkov, L. F. Chibotaru and M. Murugesu, *J. Am. Chem. Soc.*, 2014, **136**, 8003–8010.
32 J. D. Rinehart and J. R. Long, *Chem. Sci.*, 2011, **2**, 2078–2085.
33 N. F. Chilton, D. Collison, E. J. McInnes, R. E. Winpenny and A. Soncini, *Nat. Commun.*, 2013, **4**, 2551.
34 A. Borah, J. Saha, S. Sharma, S. Chaudhary, S. K. Gupta, G. Rajaraman, C. Subramaniam and R. Murugavel, *ACS Catal.*, 2023, **13**, 8535–8550.
35 A. A. Dar, S. Sen, S. K. Gupta, G. N. Patwari and R. Murugavel, *Inorg. Chem.*, 2015, **54**, 9458–9469.
36 K. Sharma, S. K. Gupta, A. Borah and R. Murugavel, *Chem. Commun.*, 2019, **55**, 7994–7997.
37 M. Llunell, D. Casanova, J. Cirera, J. Bofill, P. Alemany and S. Alvarez, *SHAPE (Version 2.1)*, Barcelona, 2013.
38 W. Zhao, H. Cui, X.-Y. Chen, G. Yi, L. Chen, A. Yuan and C.-L. Luo, *Dalton Trans.*, 2019, **48**, 5621–5626.
39 L. F. Chibotaru and L. Ungur, *Chem. Phys.*, 2012, **137**, 064112.
40 D.-Q. Wu, D. Shao, X.-Q. Wei, F.-X. Shen, L. Shi, Y.-Q. Zhang and X.-Y. Wang, *Dalton Trans.*, 2017, **46**, 12884–12892.
41 K. Soussi, J. Jung, F. Pointillart, B. Le Guennic, B. Lefeuvre, S. Golhen, O. Cador, Y. Guyot, O. Maury and L. Ouahab, *Inorg. Chem. Front.*, 2015, **2**, 1105–1117.
42 M. E. Boulon, G. Cucinotta, J. Luzon, C. Degl'Innocenti, M. Perfetti, K. Bernot, G. Calvez, A. Caneschi and R. Sessoli, *Angew. Chem., Int. Ed.*, 2013, **52**, 350–354.